Statistics of clustered vortices in the inverse energy cascade of two-dimensional turbulence

B. H. Burgess*

Centre for Atmospheric Science, Department of Earth and Environmental Sciences, The University of Manchester, Manchester M13 9PL, United Kingdom

(Received 13 October 2019; revised 15 September 2022; accepted 22 September 2022; published 31 October 2022)

The statistics of clustered and free long-lived vortices in the inverse energy cascade of forced-dissipative two-dimensional turbulence are studied. Like-sign vortices are defined as *clustered* if they are found in a contiguous region bounded by a level set of the stream function. If this region in addition contains no vortices of the opposite sign, then the cluster is *perfectly polarized*. Vortices outside these regions are *free*. The vortices found in perfectly polarized clusters exhibit a scale-invariant distribution of areas, with number density $n(A) \sim A^{-1}$, while the free number density scales as $n(A) \sim A^{-3}$. Allowing clusters to contain vortices of the opposite sign results in a progressive loss of the A^{-1} scaling as the polarization threshold is relaxed. The number of vortices in perfect clusters decreases in time via merger, while the number of free vortices increases as smaller vortices are ejected from clusters into the surrounding flow. Large clusters containing many vortices are preferentially disassembled by the vortex motions, their number decreases more quickly, and they exhibit different scaling laws than smaller clusters, which contain fewer and stronger vortices. A semiempirical mean-field theory is developed for the vortices in perfectly polarized clusters and is consistent with their observed statistics as long as small and large clusters are considered separately. As with the vortices, the cluster properties vary with scale, and this variation must be accounted for when developing a theory. The evolution of the vortex population in the forced-dissipative inverse energy cascade is found to involve two processes: the concentration of a constant amount of coherent enstrophy into a smaller and smaller fraction of the domain, and the simultaneous randomization of the surrounding flow as evidenced by decreasing polarization.

DOI: 10.1103/PhysRevFluids.7.104612

I. INTRODUCTION

Long-lived intense vortices emerge generically from random initial vorticity fields in both forced-dissipative and freely decaying two-dimensional turbulence [1–13], forming a prominent and energetically dominant flow component. Spatial hierarchies of vortices were first observed in freely decaying two-dimensional turbulence [3], and the vortex area distribution was subsequently shown to be scale-invariant [14], with more general scaling behavior [15] arising depending on the initial energy spectrum.

The long-lived vortices that populate the inverse energy cascade of forced two-dimensional turbulence have also recently been discovered to exhibit spatiotemporal scaling behavior [16,17],

*bhelenburgess@gmail.com

showing that vortices in this system not only grow in area to become much larger than the forcing scale but also exhibit nontrivial power-law scaling in space and time. Specifically, the number density distribution $n(A, t)$ of vortices with area A has three scaling ranges, with $n(A) \sim A^{-3}$ at small scales, a scale-invariant area distribution $n(A) \sim A^{-1}$ at intermediate scales, and a steep range at large scales in which $n(A) \sim A^{-6}$ [16].

The discovery of complex scaling behavior in the vortices of forced-dissipative two-dimensional turbulence offers a new window into the inverse energy cascade. One particularly interesting question regards the spatial organization of the vortices in the number density's three scaling ranges, and whether vortices in different ranges are found in distinct flow regions. However, the number density $n(A, t)$ is a domain-integrated quantity, which offers no information about where vortices are located in the flow, how they are arranged relative to each other, and how this might differ between the scaling ranges. This paper begins to answer these questions by dividing the vortex population into clustered vortices and free (unclustered) vortices, and studying their statistics and distributions across scales. Clustering of at least two vortices is a necessary precursor to merger, so this is a natural first step in studying a population in which the typical vortex area continually grows. A group of same-sign vortices is defined as *clustered* if they are located within a contiguous region bounded by a level set of the stream function. If this region in addition contains no opposite-sign vortices, then the cluster is *perfectly polarized*, containing vortices of only one sign. Vortices outside these regions are defined as *free*. As shown below, clustered and free vortices exhibit markedly different statistics and number density distributions.

The plan of the paper is as follows: Section II reviews existing theories for vortices in both freely evolving and forced two-dimensional turbulence. Particular emphasis is placed on mean-field theories for vortices in the freely decaying system and on spatial hierarchies of vortices in both decaying and forced-dissipative two-dimensional turbulence. Section III describes the numerical simulations, and Sec. IV the vortex and cluster identification algorithms. The number density distributions of clustered and free vortices are discussed in Sec. VI, and their sensitivity to cluster polarization is explored. In Sec. VII a semiempirical mean-field theory is developed for the vortices in perfect clusters, and the dependence of scaling behavior on cluster size is studied. Section VIII concludes with a summary and discussion of the most important findings and an outlook for further research.

II. THEORETICAL BACKGROUND

Two-dimensional flow with vorticity $\omega = -\nabla^2\psi$ and stream function ψ is governed by

$$\partial_t \omega + J(\psi, \omega) = f + d, \tag{1}$$

where $J(\psi, \omega)$ is the two-dimensional Jacobian, f is forcing, and d is dissipation. When initialized with spatially random vorticity fields the freely decaying system ($f = 0$) develops hierarchies of coherent vortices [3–5,14,15], which dominate the dynamics at late times, when the incoherent sea of vorticity between the long-lived vortices has undergone filamentation and been removed by dissipation.

The coherent vortices of freely decaying two-dimensional turbulence have been studied extensively in numerical simulations [5,6,14,15,18–25] and laboratory experiments [23,26–28], and a variety of theories have been proposed to predict their statistics with varying success [14,15,19,22,25,29–34]. Carnevale *et al.* [30] developed a scaling theory for vortices in the freely decaying system that assumes vortex mergers conserve energy $E \propto \mathcal{D}^{-1} \sum_i (\omega_i^{\text{ext}} A_i)^2$, where ω_i^{ext} and A_i are the vorticity extremum and area of the ith vortex, respectively, and $\mathcal{D}$ is the area of the domain, and that the vorticity extremum ω^{ext} is preserved during mergers, consistent with what is observed in numerical simulations [5]. They made a mean-field approximation, i.e., replaced ω_i^{ext} and A_i by their averages $\overline{\omega}^{\text{ext}}$ and $\overline{A}$ over the vortex population, which yields the mean-field energy

$$E \sim \rho(\overline{\omega}^{\text{ext}}\overline{A})^2 \sim \rho\overline{\Gamma}^2 = \text{constant}, \tag{2}$$

where $\rho \equiv N/\mathcal{D}$ is the vortex density and N is the number of vortices. Assuming the vortex density $\rho \sim t^{-\chi}$ and using conservation of energy and of the vorticity extremum they predicted the growth rates of the average vortex circulation $\overline{\Gamma}(t) \sim t^{\chi/2}$ and vortex area $\overline{A}(t) \sim t^{\chi/2}$ and the enstrophy decay rate $Z(t) \sim t^{-\chi/2}$. Carneval *et al.* had no prediction for χ, but subsequent mean-field approaches predicted $\chi = 1$ [22,33] and $\chi = 2/3$ [34].

Lacasce [25] measured the absolute dispersion of the vortices in numerical simulations of freely decaying two-dimensional turbulence and showed that the mean vortex circulation $\overline{\Gamma}(t)$ increased at the same rate as the diffusivity $D \sim \overline{\Gamma}(t) \sim t^{1/3}$. Assuming the mean-field energy $E \sim \rho\overline{\Gamma}^2 =$ constant and taking a semiempirical approach by using the measured growth rate of the circulation $\overline{\Gamma}(t) \sim t^{1/3}$ he predicted $\rho \sim t^{-2/3}$, i.e., $\chi = -2/3$. He also generalized the approach to nonconservative simulations in which the choice of dissipation mechanism caused the mean vortex amplitude to decay and the vortex area to increase.

Benzi *et al.* [3], Dritschel *et al.* [14], and Burgess *et al.* [15,35] went beyond the mean-field approaches described above and considered the distribution of vortex areas A_i in freely decaying two-dimensional turbulence. In numerical simulations Benzi *et al.* [3] observed a self-similar distribution of coherent structures, and the number of vortices with radius R followed a power-law distribution $n(R) \sim R^{-\alpha}$ with $\alpha \approx 1.90$. Dritschel *et al.* [14] fixed the A-dependence of the number density $n(A) \sim A^{-1}$ by requiring a scale-invariant distribution of vortex areas. They assumed vortices contain almost all the energy E, and that the vortex mean-square vorticity $\overline{\omega_{\rm v}^2}$ is independent of vortex area A and time t, where

$$\overline{\omega_{\rm v}^2} \equiv \frac{1}{N}\sum_{i=1}^{N}\frac{1}{A_i}\int_{A_i}\omega^2 d\mathbf{x}, \tag{3}$$

and N is the number of vortices. Further requiring a scale-invariant enstrophy decay rate, they predicted $n(A,t) \sim t^{-2/3}A^{-1}$, $A(t) \sim t^{1/3}$, and $Z(t) \sim t^{-1/3}$, which has been verified for numerical simulations starting from top-hat initial energy spectra [15]. Burgess *et al.* [15] subsequently showed that the scaling of the freely decaying vortex number density depends on the initial conditions. Even in this case, however, the number density compensated by $\overline{\omega_{\rm v}^2}$ assumes a self-similar form $n(A)/\overline{\omega_{\rm v}^2}(A,t) \sim t^{-2/3}A^{-1}$.

Strong, long-lived vortices also populate the inverse energy cascade of forced-dissipative two-dimensional turbulence when the forcing scale is sufficiently well-resolved [7–10,12,13], but much less work has focused on this system. Burgess and Scott [16] developed a scaling theory for these vortices assuming constant energy injection, such that $E \sim t$. Using $Z =$ constant at inverse cascade scales, they predicted vortex areas would grow like

$$A(t) \sim E/Z \sim t, \tag{4}$$

and postulated a three-part number density consisting of a small-scale range equilibrated with the forcing, an intermediate scale-invariant range in which $n(A) \sim A^{-1}$, and a large-scale steep range populated by few and strong vortices. Using the concept of transport of a conserved quantity across scales, as in turbulent inertial ranges, they postulated that the quantities $E_{\rm v} \equiv (2\mathcal{D})^{-1}\int \overline{\omega_{\rm v}^2}A^2 n(A)dA$, $Z_{\rm v} \equiv (2\mathcal{D})^{-1}\int \overline{\omega_{\rm v}^2}An(A)dA$, and $\sigma_{\rm v} \equiv (2\mathcal{D})^{-1}\int \overline{\omega_{\rm v}^2}n(A)dA$ would be conserved in "comoving" intervals $[\mu A_0(t), A_0(t)]$, where $0 < \mu < 1$ is a constant, in the small-, intermediate-, and large-scale ranges, respectively. The quantities $E_{\rm v}$, $Z_{\rm v}$, and $\sigma_{\rm v}$ are a vortex self-energy, enstrophy, and a mean-square-vorticity-weighted vortex number, respectively, where note that $n(A)dA = dN$ and N is the number of vortices. Comoving intervals have endpoints that evolve at the area growth rate given by Eq. (4), and their use enforces conservation in an evolving range of scales that grows at the same rate as the energy-containing length scale. Using $A_0(t) \sim t$,

and allowing for a time-varying vortex mean-square vorticity led to the prediction

$$n(A,t) \sim \begin{cases} A^{-3}, & A_f \leqslant A < A_-, \\ \overline{\omega_{\rm v}^2}^{-1} t^{-1} A^{-1}, & A_- < A < A_+, \\ \overline{\omega_{\rm v}^2}^{-1} t^{r_3-1} A^{-r_3}, & A_+ < A \leqslant A_{\rm max}, \end{cases} \tag{5}$$

which was verified in high-resolution simulations, with r_3 measured to be $r_3 \approx 6$.

The number density in Eq. (5) contains no information about the spatial location of the vortices in the three scaling ranges. This paper seeks to remedy that omission by providing insight into how the spatial organization of the vortex population is related to the scaling observed in the number density. To approach the problem, note that vortices in this system grow in area through merger, and that the number density decays as $\overline{\omega_{\rm v}^2}^{-1} t^{-1}$ in the scale-invariant intermediate range where $n(A) \sim A^{-1}$. Since the intermediate range decays, vortices in this range must be undergoing merger, such that their number falls off in time. Secondly, note that clustering of at least two like-sign vortices is a necessary precursor to merger. These considerations lead to the prediction, tested below, that the scale-invariant area distribution will be found among like-sign vortices grouped together in clusters.

A second goal of this paper is to study how well a mean-field approach can predict the statistics and scaling properties of clustered vortices in this system, which contains a wide range of vortex sizes with statistical properties that depend on scale. The forced-dissipative flow considered here is what LaCasce [25] would call nonconservative, because the energy and vortex mean-square vorticity $\overline{\omega_{\rm v}^2}$ grow continually [16]. (The vortex mean-square vorticity $\overline{\omega_{\rm v}^2}$ will play the role of by vortex peak vorticity in the mean-field theories for the freely decaying system discussed above.) This poses in principle no problem for a mean-field theory. A more likely impediment is that the characteristics of vortices, and of the clusters they form, vary with scale, and averaging over subpopulations with different statistical characteristics will yield unexpected results. Hence, appropriately selecting subpopulations will be key to developing a consistent mean-field theory.

III. NUMERICAL SIMULATIONS

Forced-dissipative flows governed by Eq. (1) are simulated with a pseudospectral method in a doubly periodic domain of side lenth $L = 2\pi$ at resolution 8192^2 grid points. The forcing is δ-correlated in time and narrow-band in spectral space, centered on wave number $k_f = 1024$. The initial condition is a state of no flow, and the energy injected over one time step is $\varepsilon_I dt$, with $\varepsilon_I = 1$, such that energy $E \sim t$. Once the flow is well-developed 78% of the injected energy cascades toward large scales. A spectral filter [36] is used for dealiasing, giving a maximum resolved wave number $k_m = 3N/8$; here $N = 8192$ and $k_m = 3072$.

Fourth-order hyperviscous dissipation is used at small scales, but there is no large-scale drag or hypoviscosity. The lack of large-scale dissipation means the inverse cascade is in a quasisteady state, in which the energy spectrum is approximately stationary over a wide range of scales, while the spectral peak continually moves to larger scales. Further details on the simulations can be found in Ref. [16].

IV. VORTEX AND CLUSTER IDENTIFICATION

To identify clusters, intense vortices are first extracted from the flow field, and then clusters of same-sign vortices grouped together within level sets of the stream function are identified. Vortices are extracted using the procedure described in Ref. [17], which finds contiguous regions containing intense concentrations of vorticity exceeding a threshold $\omega_{\rm thr}$. A shifting cutoff based on the root-mean-square (rms) vorticity is used. Bartello and Warn [37] found shifting cutoffs preferable for identifying vortices, and LaCasce [25] found they yielded mean-field estimates for energy and enstrophy that better approximated the actual values and observed decay rate. Here the threshold is set to $\omega_{\rm thr} = 1.5\omega_{\rm rms}$ as in Ref. [17]. To be a vortex, each contiguous region must

also have a peak vorticity $\omega_{\rm p}$ exceeding a second threshold, $\omega_{\rm p} > \omega_{\rm thr}^{\rm p}$, where $\omega_{\rm thr}^{\rm p} = 4\omega_{\rm rms}$. This eliminates regions that lack the intense peak possessed by long-lived vortices. Combining the two thresholds, the resulting vortex field $\omega_{\rm v}$ satisfies

$$\omega_{\rm v} = \begin{cases} \omega, & |\omega| \geqslant 1.5\omega_{\rm rms} \text{ and } |\omega_{\rm p}| \geqslant 4\omega_{\rm rms}, \\ 0, & |\omega| < 1.5\omega_{\rm rms} \text{ and/or } |\omega_{\rm p}| < 4\omega_{\rm rms}. \end{cases} \tag{6}$$

Once $\omega_{\rm v}$ has been extracted, a multilevel thresholding procedure is used to scan through the stream-function field and find vortex clusters. The procedure starts by selecting all regions on which $\psi > 0$, and then successively identifies contiguous regions on which $\psi \geqslant m\Delta|\psi|$, where the level index $m \in 1, \ldots, N_{\rm lev} - 1$, and m starts at 1. The increment $\Delta|\psi| = |\psi|_{\rm max}/N_{\rm lev}$, where $|\psi|_{\rm max}$ is the maximum value taken by $|\psi|$ on the domain and $N_{\rm lev}$ is the number of levels. There was little difference in the results between $N_{\rm lev} = 100$ and $N_{\rm lev} = 1000$. Within each contiguous region identified for a given threshold $m\Delta|\psi|$ the number of vortices signed oppositely to ψ and the number of vortices with the same sign as ψ are counted. A region must contain at least two vortices antialigned with ψ to qualify as a cluster. To find the cluster polarization, the absolute coherent circulation

$$\Gamma_{\rm v}^{\rm cl} = \sum_{i=1}^{N^+} |\mathbf{\Gamma}_i^+| + \sum_{i=1}^{N^-} |\mathbf{\Gamma}_i^-| \tag{7}$$

is first calculated, where N^+ and N^- are the number of positive and negative vortices in the cluster, respectively, and $\mathbf{\Gamma}_i^+$ and $\mathbf{\Gamma}_i^-$ are the circulations of the ith positive and negative vortex. Note that the absolute values of the circulations are summed to avoid cancellations between positive and negative vortices, so $\Gamma_{\rm v}^{\rm cl}$ is a positive quantity. To set a threshold on polarization, vortices of the dominant sign (i.e., the sign antialigned with ψ in that region) are then required to make a minimum contribution to $\Gamma_{\rm v}^{\rm cl}$. The requirement is

$$P_\Gamma \equiv \frac{\sum_{i=1}^{N^\pm} |\mathbf{\Gamma}_i^\pm|}{\Gamma_{\rm v}^{\rm cl}} \geqslant P_{\rm thr}, \tag{8}$$

where the positive (negative) sign is taken if the cluster is dominated by positive (negative) vortices. If the region passes the polarization test, then it is removed from the stream-function field and added to the cluster field. The clusters identified are thus the largest possible regions such that $P_\Gamma \geqslant P_{\rm thr}$, and regions are not double-counted.

The procedure is then repeated for regions with $\psi < 0$. Contiguous regions on which $|\psi| \geqslant m\Delta|\psi|$ are again identified and clusters with $P_\Gamma \geqslant P_{\rm thr}$ are extracted at each level m for $m \in 1, \ldots, N_{\rm lev} - 1$ and added to the clustered field. Because the procedure starts at a low value of $|\psi|$, the regions identified are the largest possible regions meeting the polarization threshold, and they are bounded by level sets of the stream function exceeding the set of thresholds $\psi_{\rm thr} = \{(1, 2, \ldots, N_{\rm lev} - 1)\Delta|\psi|\}$.

Stream-function regions $\psi_{\rm cl}$ for thresholds $P_{\rm thr} = 0.85, 0.9, 0.95$, and $P_{\rm thr} = 1$ are shown in Fig. 1 at $t = 4.0$. As $P_{\rm thr}$ increases, the clusters become smaller and more widely separated. The focus below will be on perfectly polarized clusters $\psi_{\rm pc}$, where the subscript "pc" stands for perfect clusters ($P_\Gamma = P_{\rm thr} = 1$), though the sensitivity of the vortex number densities and select cluster statistics to polarization will also be explored.

V. PROPERTIES OF CLUSTERS AND VORTICES

A. Cluster properties

At early times, the domain is almost filled with perfectly polarized clusters—see Fig. 2, top left, which shows $\psi_{\rm pc}$ at $t = 1.0$. As the inverse cascade proceeds, perfect clusters become more sparsely distributed, occupying a diminishing fraction of the domain, as shown in the middle left ($t = 2.0$)

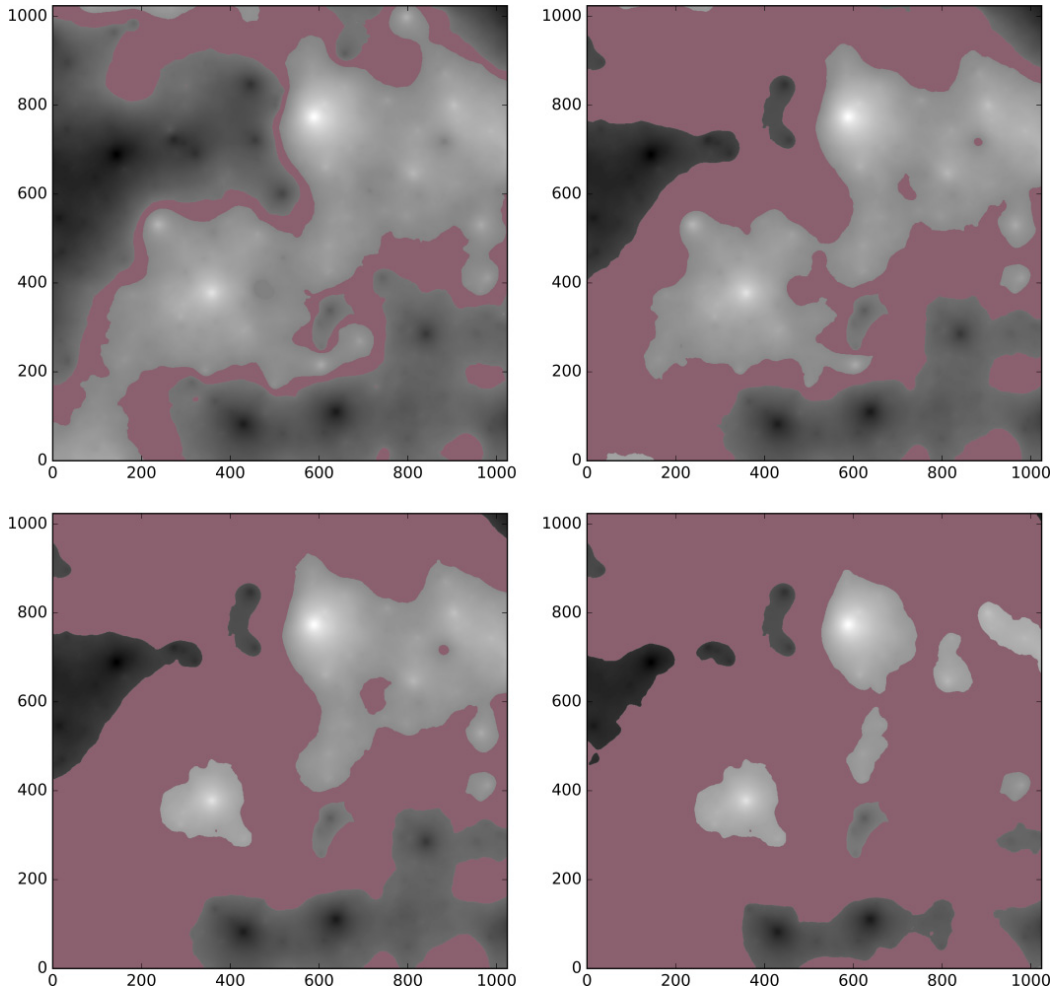

FIG. 1. Stream-function regions $\psi_{\rm cl}$ satisfying $P_\Gamma \geqslant 0.85$ (top left), $P_\Gamma \geqslant 0.9$ (top right), $P_\Gamma \geqslant 0.95$ (bottom left), and $P_\Gamma = 1.0$ (perfect clusters, bottom right) at $t = 4.0$. Light regions correspond to positive and dark regions to negative ψ. The region shown is 1/64th of the domain.

and bottom left panels ($t = 3.0$). This process reflects the evolution of the corresponding vortex population, shown in the right column of Fig. 2. As merger of like-sign vortices generates a wider range of vortex areas and strengths, large strong vortices become more sparsely distributed, as can be seen by comparing the bottom right panel, which shows the coherent vortex field at $t = 3.0$, to the top right panel, which shows the vortices at $t = 1.0$. At the same time clusters also become more widely spaced.

The amount of kinetic energy in perfectly polarized clusters $\psi_{\rm pc}$ reflects the diminishing domain fraction the clusters occupy: as shown in Fig. 3(a), at early times ($0.25 \lesssim t \lesssim 2.0$) the energy $E_{\rm pc}$ (dash-dot black line) in perfectly polarized clusters dominates the energy $E - E_{\rm pc}$ (dotted black line) outside the clusters. The curves shown here and in subsequent sections represent averaged data from an ensemble of three simulations. Note that $E_{\rm pc}$ is the sum over perfect clusters of the kinetic energy density generated by the entire vorticity distribution, including both coherent vortices and the incoherent filamentary sea. After $t \approx 0.5$ the energy $E_{\rm pc}$ in perfect clusters grows more slowly than the energy $E - E_{\rm pc}$ in the surrounding flow, which makes the dominant contribution to the total

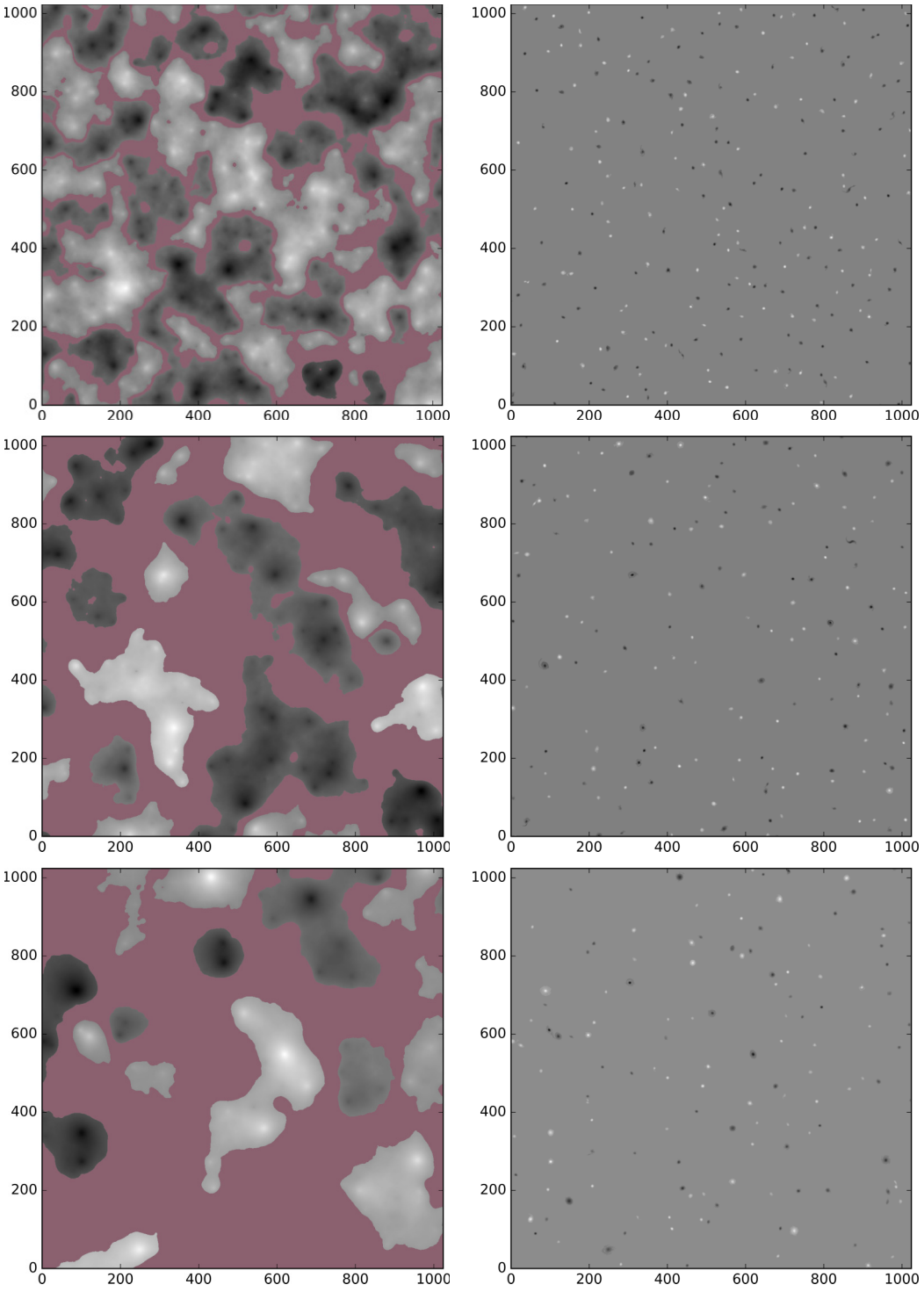

FIG. 2. Perfectly polarized ($P_\Gamma = 1.0$) stream-function regions $\psi_{\rm pc}$ (left) and corresponding coherent vortex field $\omega_{\rm v}$ (right) at $t = 1.0$ (top), $t = 2.0$ (middle), and $t = 3.0$ (bottom). Light regions correspond to positive and dark regions to negative ψ and ω. The region shown is 1/64th of the domain.

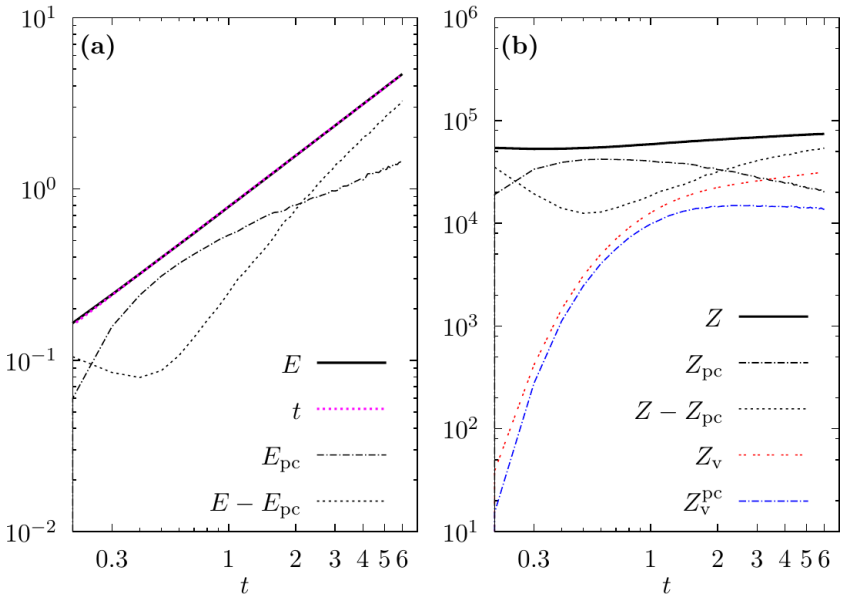

FIG. 3. (a) Total kinetic energy E (solid black line) with t (dotted magenta line) for comparison, energy $E_{\rm pc}$ (dash-dot black line) in perfectly polarized clusters, and energy $E - E_{\rm pc}$ (dotted black line) outside perfect clusters. (b) Total enstrophy Z (solid black line) enstrophy $Z_{\rm pc}$ (dash-dot black line) in perfect clusters, enstrophy $Z - Z_{\rm pc}$ (dotted black line) outside perfect clusters, total coherent enstrophy $Z_{\rm v}$ (double-dotted red line) in all vortices, and coherent enstrophy $Z_{\rm v}^{\rm pc}$ (blue dash-dot line) in perfect clusters.

energy after $t \approx 2.0$. The total kinetic energy E (solid black line) grows like t (dotted magenta line) as prescribed.

The enstrophy $Z_{\rm pc}$ in perfectly polarized clusters peaks at early times when the clusters almost fill the domain, and then falls off, as shown in Fig. 3(b) (dash-dot black line). The enstrophy $Z - Z_{\rm pc}$ outside perfect clusters (dotted black line) begins to grow at $t \approx 0.5$, making the dominant contribution to the total enstrophy after $t \approx 2.0$. Note that Z and $Z_{\rm pc}$ include both the incoherent filamentary vorticity field and the coherent vortices. The total enstrophy Z grows slowly after $t \approx 0.4$, most likely due to hyperviscous sharpening of the vortex peaks, since it is not observed in simulations with ordinary Laplacian viscosity [17].

The coherent enstrophy $Z_{\rm v}^{\rm pc}$ in perfectly polarized clusters grows at early times and then is approximately constant after $t \approx 2.0$, as can be seen in Fig. 3(b) (blue dash-dot line). Note that "coherent" indicates that only contributions from the vortex cores are included, and filamentary vorticity is excluded. The total coherent enstrophy $Z_{\rm v}$ (red double-dotted line) contained in all vortices, both free and clustered, grows until the end of the simulation. Using a lower threshold on vorticity in Eq. (6) retains more vortices in the coherent field, resulting in smaller perfectly polarized clusters occupying less of the domain. However, the trends seen in Fig. 3 are unchanged.

The percentage $f_{\rm cl}$ of the domain occupied by clusters depends on the polarization threshold $P_{\rm thr}$. (Here the subscript "cl" indicates that the cluster polarization is being allowed to vary.) As shown in Fig. 4, $f_{\rm cl}$ decreases as $P_{\rm thr}$ increases (top to bottom). For $P_{\rm thr} \in [0.8, 0.85, 0.9, 0.95, 1]$ $f_{\rm cl}$ also decreases with time. This indicates decreasing polarization of the flow around the perfectly polarized clusters: not only are the perfect clusters ($P_\Gamma = P_{\rm thr} = 1$, dark blue solid line at bottom) becoming more widely spaced, as shown in Fig. 2, left, the vortices in the flow around them are also increasingly less likely to be found in like-sign clusters and more likely to be found in dipoles and neutral groups of vortices as time goes on.

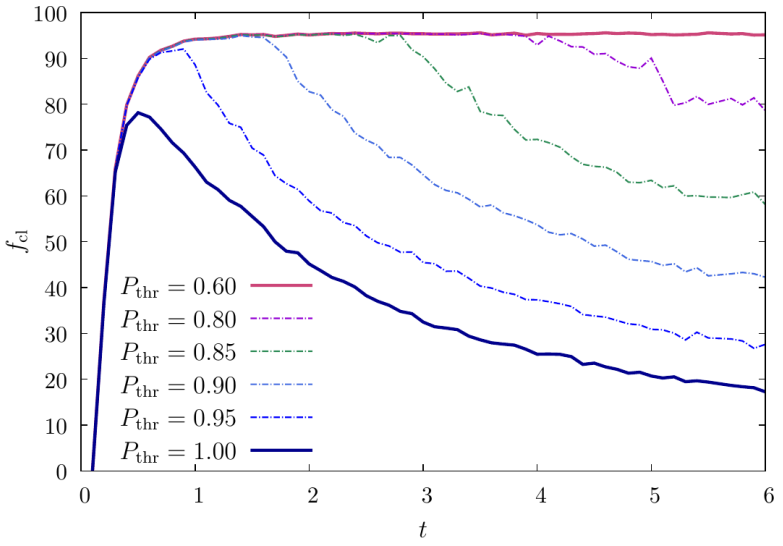

FIG. 4. Percentage $f_{\rm cl}$ of the domain occupied by clusters satisfying $P_\Gamma \geqslant P_{\rm thr}$, where $P_{\rm thr}$ is given in the legend.

Up until $t \approx 0.4$, all the domain fraction curves coincide with the perfectly polarized ($P_{\rm thr} = 1.0$) curve, which means that no matter the value of $P_{\rm thr}$, all the clusters identified up until $t \approx 0.4$ are perfectly polarized. Similarly, up until $t \approx 0.7$, when the $P_\Gamma \geqslant 0.95$ curve diverges, all clusters are at least 95% polarized, and up until $t \approx 1.8$, when the $P_\Gamma \geqslant 0.9$ curve diverges, all clusters are at least 90% polarized. The $P_\Gamma \geqslant 0.6$ polarization curve (solid dark pink line at top) saturates at about $f_{\rm cl} \approx 95\%$, and never falls off, indicating that all clusters identified over the course of the simulation have at least 60% polarization.

The domain fractions in Fig. 4 show that there is increasing disorder in the vortex population as indicated not only by decreasing polarization but also by a decreasing number of perfect clusters—see Fig. 5(a), solid dark blue line. The flow undergoes a process of "spreading neutralization," which eats away at the perfect clusters, decreasing their number and the polarization of the surrounding flow as time goes on. This process unfolds as coherent vorticity is simultaneously concentrated into larger, stronger, and more widely separated vortices. The number of clusters satisfying $P_\Gamma \geqslant P_{\rm thr}$ for all choices of $P_{\rm thr}$ peaks at a time that varies with polarization, as shown in Fig. 5(a). All curves initially follow the $P_\Gamma \geqslant 0.6$ polarization curve and then subsequently diverge from it, with the $P_\Gamma = 1.0$ curve diverging first at $t \approx 0.3$. In general, the number of clusters increases with polarization, because raising $P_{\rm thr}$ breaks large weakly polarized regions into smaller sub-groups of predominantly like-sign vortices. The decline in the number of clusters with $P_\Gamma \geqslant 0.6$ after $t \approx 0.8$ is due to the inverse cascade and the growing length scale of the stream function. This is confirmed by the average area per cluster shown in panel (b), which increases for clusters with $P_\Gamma \geqslant 0.6$, showing that weakly polarized clusters grow larger as the inverse cascade proceeds.

The decline in the number of clusters with higher levels of polarization, however, is tied to the increasing disorder and neutrality of the flow, i.e., the process of "spreading neutralization" described above, and the simultaneous concentration of coherent vorticity into fewer and larger vortices. As shown in Fig. 5(b) the more strongly polarized clusters have roughly constant average area per cluster despite the growth in the energy-containing length scale driven by the inverse energy cascade. This is particularly clear for the perfectly polarized ($P_\Gamma = 1.0$, solid dark blue curve) and 95% polarized ($P_\Gamma \geqslant 0.95$, dash-dot blue curve) clusters. Lower polarizations have noisier curves, due to a smaller sample size.

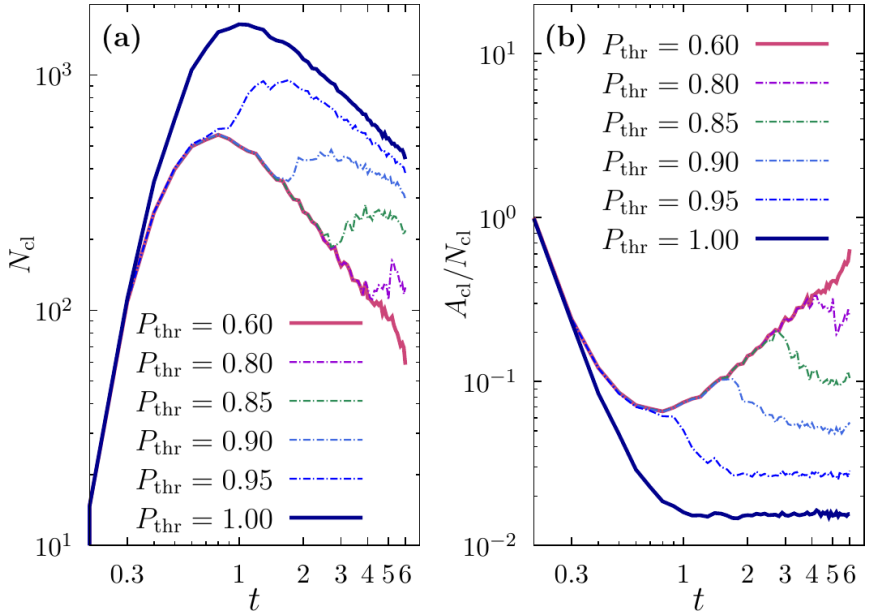

FIG. 5. (a) Number $N_{\rm cl}$ of clusters satisfying $P_\Gamma \geqslant P_{\rm thr}$. (b) Average area per cluster $A_{\rm cl}/N_{\rm cl}$ satisfying $P_\Gamma \geqslant P_{\rm thr}$, where $P_{\rm thr}$ is given in the legend.

B. Properties of clustered and free vortices

The number of clustered vortices $N_{\rm v}^{\rm pc}$ (black dash-dot line) found in perfectly polarized clusters with $P_\Gamma = 1.0$ increases until $t \approx 0.8$ and then decreases, with a power-law decay of $N_{\rm v}^{\rm pc} \sim t^{-1.18\pm0.02}$ on the interval $1.5 < t < 6.0$, as shown in Fig. 6(a). The decrease is due to ongoing mergers within the clusters and ejection of clustered vortices into the free population. The number of free vortices outside perfect clusters $N_{\rm v} - N_{\rm v}^{\rm cl}$ (black dotted line) increases continually, with $N_{\rm v} - N_{\rm v}^{\rm cl} \sim t^{0.20\pm0.01}$ on the interval $1.5 < t < 6.0$.

The total area $A_{\rm v}$ occupied by all vortex cores in the flow increases until $t \approx 1.0$ and then is roughly constant thereafter, as shown in Fig. 6(b) (solid black line). The area $A_{\rm v}^{\rm pc}$ (black dash-dot line) occupied by vortex cores in perfectly polarized clusters increases until $t \approx 1.0$ and then falls off, with a power-law decay of $A_{\rm v}^{\rm cl} \sim t^{-0.51\pm0.01}$ on the interval $1.5 < t < 6.0$. This decrease occurs primarily due to ejection of clustered vortices into the surrounding flow and, to a lesser extent, filament shedding during mergers. The area occupied by free vortex cores $A_{\rm v} - A_{\rm v}^{\rm cl}$ (black dotted line) grows like $t^{0.43\pm0.01}$ due to ejection of vortices from the perfect clusters.

In both populations of vortices, clustered and free, the average enstrophy per vortex increases, as shown in Fig. 6(c). The enstrophy per vortex grows more slowly for the free vortices than in the clustered population. Least-squares fits are given to quantify the growth rate at later times, although it is evident that these quantities do not grow as power laws.

The average area of a clustered vortex core $\overline{A_{\rm v}^{\rm pc}} = A_{\rm v}^{\rm pc}/N_{\rm v}^{\rm pc}$ (black dash-dot line) grows, with $\overline{A_{\rm v}^{\rm pc}} \sim t^{0.67\pm0.01}$ on the interval $1.5 < t < 6.0$. The average area of a free vortex core $\overline{A_{\rm v} - A_{\rm v}^{\rm pc}} = (A_{\rm v} - A_{\rm v}^{\rm pc})/(N_{\rm v} - N_{\rm v}^{\rm pc})$ (black dotted line), also grows, but more slowly, with $\overline{A_{\rm v} - A_{\rm v}^{\rm pc}} \sim t^{0.24\pm0.01}$ on the interval $1.5 \leqslant t \leqslant 6.0$. The different growth rates indicate that smaller vortices are preferentially ejected from perfect clusters and larger free vortices preferentially join them.

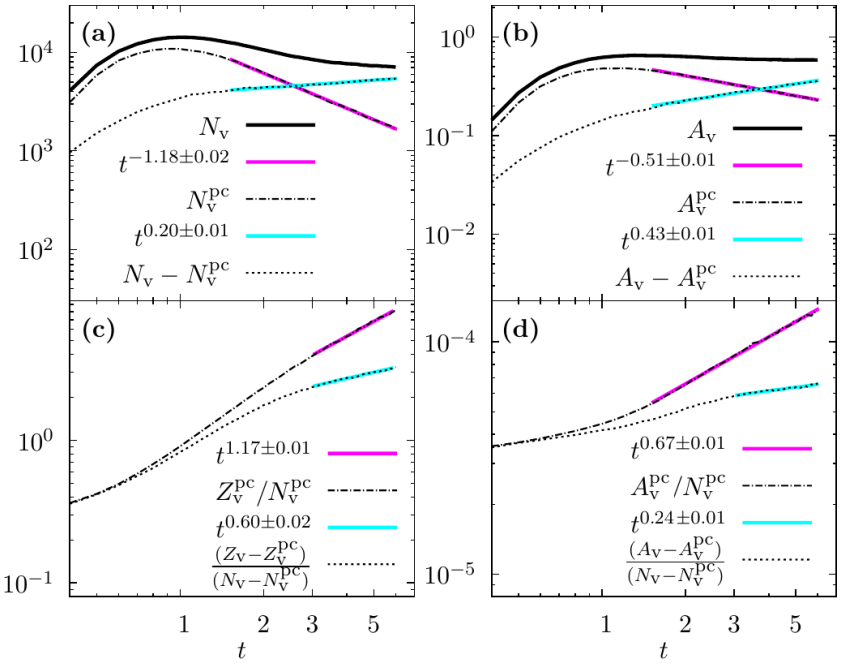

FIG. 6. (a) Number of vortices N_v^{pc} (dash-dot black line) in perfect clusters, and number of free vortices $N_v - N_v^{pc}$ (dotted black line) outside perfect clusters, where N_v is the total number of vortices. (b) Total coherent (core) area A_v^{pc} (dash-dot black) of clustered vortices and of free vortices, $A_v - A_v^{pc}$ (dotted black), where A_v is the total core area of all vortices. (c) Average enstrophy Z_v^{pc}/N_v^{pc} (dash-dot black) of a clustered vortex, and of a free vortex, $(Z_v - Z_v^{pc})/(N_v - Z_v^{pc})$ (dotted black). (d) Average core area A_v^{pc}/N_v^{pc} (dash-dot black) of a clustered vortex, and of a free vortex, $(A_v - A_v^{pc})/(N_v - N_v^{pc})$ (dotted black). Least-squares fit lines are magenta and cyan.

VI. CLUSTERED AND FREE VORTEX NUMBER DENSITY DISTRIBUTIONS

The number of vortices as a function of area and time, i.e., the number density distribution, differs between the clustered and free populations, as shown in Fig. 7. The free number density, shown in Fig. 7(a) at $t = 3.0,\ 4.5,\ 6.0$, follows the scaling $n_f(A) \sim A^{-3}$ over the equilibrated range $-4.45 \lesssim \log_{10}(A) \lesssim -4$, in which the number of vortices does not change in time. The power law shallows in the range $-4 \lesssim \log_{10}(A) \lesssim -3.8$, where the number density also falls off in time, suggesting this range is tending toward the A^{-3} scaling already established at smaller scales. The free number density is farthest out of equilibrium at large scales, where the number of vortices increases in time as $n_f(A, t)$ extends to larger scales. This reflects the escape of large vortices generated via merger in the clusters into the free population in the surrounding flow.

The number density distribution $n_{pc}(A, t)$ of clustered vortices in perfect clusters, which is shown in Fig. 7(b) at the same three times $t = 3.0,\ 4.5,\ 6.0$, exhibits markedly different scaling, with $n_{pc}(A, t) \sim A^{-1}$ over a range that moves to larger scales in time. At $t = 3.0$ this range extends from $\log_{10}(A) \approx -4.3$ to $\log_{10}(A) \approx -3.7$, while at $t = 6.0$ it extends from $\log_{10}(A) \approx -4.2$ to $\log_{10}(A) \approx -3.6$. The clustered number density steepens at smaller scales, possibly because vortex merger inevitably generates both large and small vortices [38], and the latter then build up at small scales. Like the free number density, the clustered number density extends to larger scales in time, again because merger generates increasingly large vortices. The range of vortex areas present in the free A^{-3} range and the clustered A^{-1} range overlap, showing that the power law depends not only on scale but also location relative to the other vortices in the flow.

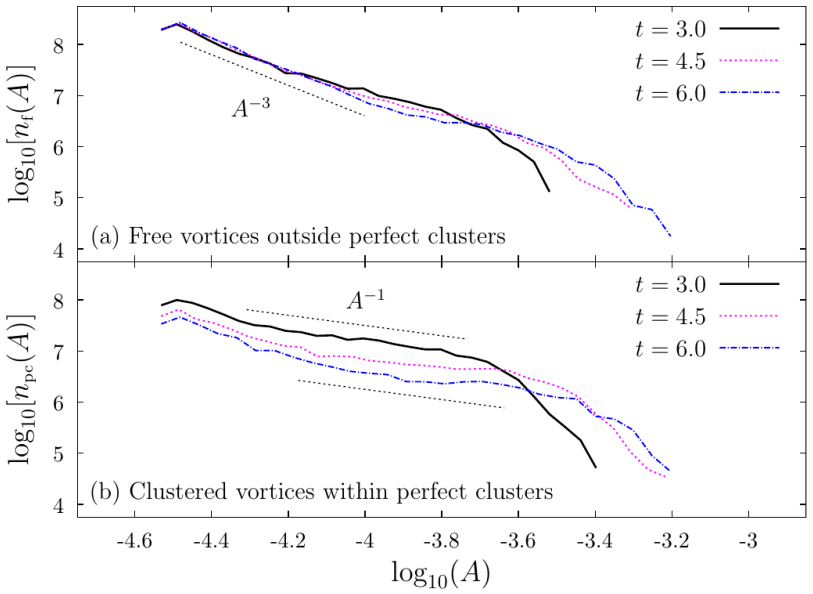

FIG. 7. Number density distributions of (a) free vortices outside perfect clusters, with A^{-3} scaling line, and (b) vortices in perfect clusters, with A^{-1} scaling lines.

The impact of polarization threshold $P_{\rm thr}$ on the clustered number density is explored in Fig. 8, which shows the density at $t = 3.0$ for various choices of $P_{\rm thr}$. For perfectly polarized clusters with $P_\Gamma = 1.0$ the number density follows a scale-invariant area distribution $n_{\rm pc}(A) \propto A^{-1}$ over $[-3.8 \lesssim \log_{10}(A) \lesssim -4.35]$. As $P_{\rm thr}$ decreases, the curve steepens and the A^{-1} scaling is lost. Hence, the power law is sensitive to cluster polarization, and the scale-invariant area distribution is associated with vortices in perfectly polarized clusters.

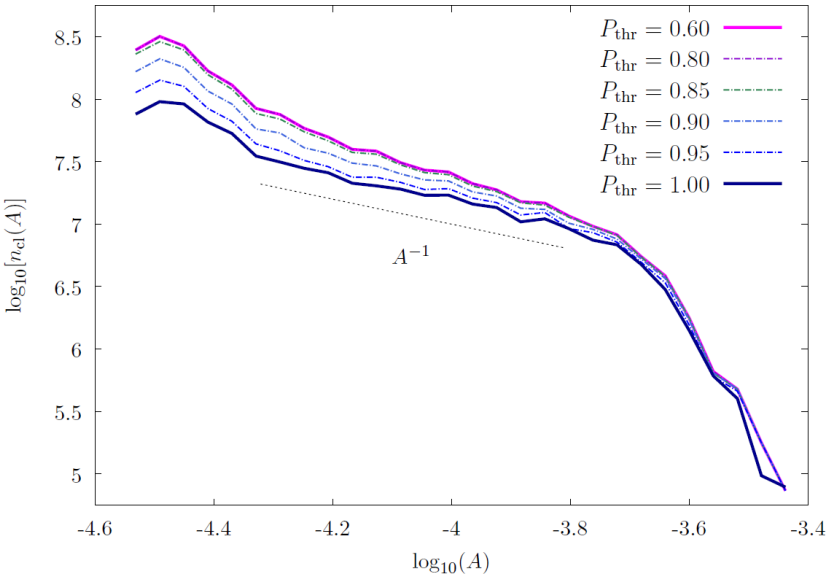

FIG. 8. Number density distribution of vortices in clusters satisfying $P_\Gamma \geqslant P_{\rm thr}$ at $t = 3.0$.

VII. A MEAN-FIELD THEORY FOR THE CLUSTERED VORTICES

The simplest approach to developing a theory for vortex statistics is to attempt to predict mean quantities, such as the growth rate of an average vortex area and the decay rate of the number of vortices, without accounting in detail for all the complex interactions affecting the vortex population. Such a mean-field theory approach [39] has been used previously for vortices in freely decaying two-dimensional turbulence by Carnevale *et al.* [30], Pomeau [33], Sire and Chavanis [22], Iwayama [34], and LaCasce [25], for example. LaCasce in particular generalized the mean-field approach to nonconservative numerical experiments using arguments that did not assume conservation of energy or of the vortex amplitude. The present simulations are clearly nonconservative on two counts: because the system is forced the energy grows, $E \sim t$, and the vortex mean-square vorticity similarly increases, with $\overline{\omega_{\rm v}^2} \sim (\overline{\omega}_{\rm v})^2 \sim t^{1/3}$ in the A^{-1} range, as found by Burgess and Scott [16].

To develop a mean-field theory for the clustered vortices, begin by ignoring the distribution of vortex areas and strengths and considering the length scale $\ell(t) \sim \sqrt{E/Z}$. This length appears in Kraichnan's treatment of the equilibrium statistics of two-dimensional flow [40], where the value of $k_{\rm I}^2 \equiv Z/E$ partially determines which of three thermal equilibrium regimes the system is in. Thompson and Young [41] identified $\ell(t)$ with the core radius of a barotropic vortex in a two-mode f-plane quasigeostrophic model. Burgess and Scott [16] similarly identified $\ell(t)$ with the vortex core radius in the forced-dissipative inverse cascade, and showed that the area of the largest vortex grew like $A_{\rm max} \sim \ell^2(t) \sim t$, where $E \sim t$ was specified by the choice of forcing and $Z =$ constant for the inverse cascade.

Before proceeding, it is helpful to revisit the interpretation of $\ell(t)$, specialising to perfectly polarized clusters, for which a mean-field theory is sought. Let $E_{\rm pc}$ and $Z_{\rm v}^{\rm pc}$, where "pc" stands for "perfect cluster" and "v" denotes a quantity associated with vortex cores, be the total energy and coherent enstrophy contained in perfectly polarized clusters, and

$$\ell(t) = 2\pi \sqrt{\frac{E_{\rm pc}}{Z_{\rm v}^{\rm pc}}}. \tag{9}$$

Equation (9) implies

$$E_{\rm pc} \;=\; \frac{1}{4\pi^2}\,\ell^2(t) Z_{\rm v}^{\rm pc} \;=\; \frac{1}{4\pi^2}\ell^2(t) N_{\rm v}^{\rm pc} \overline{A}(t) \overline{\omega_{\rm v}^2}(t), \tag{10}$$

where $\overline{A}(t)$ is the mean area of a clustered vortex (the scripts "pc" and "v" have been omitted to simplify the notation), $Z_{\rm v}^{\rm pc} = N_{\rm v}^{\rm pc} \overline{A}(t) \overline{\omega_{\rm v}^2}(t)$, and $\mathcal{D} = 4\pi^2$ is the area of the domain. Note that $\overline{A}(t)$ need not grow in the same way as the largest vortex area $A_{\rm max}(t)$; in fact, if the average of A is taken over a range in which vortices are undergoing merger, which generically produces both larger and smaller vortices [38], then $\overline{A}(t)$ will grow more slowly than $A_{\rm max}(t)$. Now, as shown in Fig. 9(a) the vortex mean vorticity $\overline{\omega}_{\rm v} \sim t^{1/6}$ after $t \approx 3.5$ in these simulations, so $\overline{\omega_{\rm v}^2} \sim (\overline{\omega}_{\rm v})^2 \sim t^{1/3}$. Hence, one can replace $\overline{A}(t)\overline{\omega_{\rm v}^2}(t)$ with $\overline{\Gamma}(t)\overline{\omega}(t)$, where $\overline{\Gamma}(t) = \overline{A}(t)\overline{\omega}(t)$ is the mean circulation of a clustered vortex. This yields

$$E_{\rm pc} \;=\; \frac{1}{4\pi^2} N_{\rm v}^{\rm pc} \times \overline{\Gamma}(t)\overline{\omega}(t) \times \ell^2(t) \;=\; \frac{1}{4\pi^2} N_{\rm v}^{\rm pc} \times uL/T \times \ell^2(t) = \frac{1}{4\pi^2} N_{\rm v}^{\rm pc} \times u^2 \times \ell^2(t). \tag{11}$$

Here $\overline{\Gamma}(t) = \overline{A}(t)\overline{\omega}(t) = uL$ is the average circulation of a clustered vortex, where u is tangential speed and L an average vortex perimeter, and $\overline{\omega}(t) = 1/T$ is a vortex turnaround time. If the mean-field estimate for the cluster energy $E_{\rm pc}$ is correct, then Eq. (11) implies that $\ell^2(t)$ must be the area over which an average vortex generates a strong flow velocity and contribution to the kinetic energy. This region is larger than the vortex core, but grows the same way. The growth rate of $E_{\rm pc}$ in Fig. 9(b) will be discussed below.

Identifying $\ell^2(t)$ not with the vortex core but with the flow region dominated by the swirling velocity field generated by the vortex allows the total area $A_{\rm pc}$ occupied by perfectly polarized

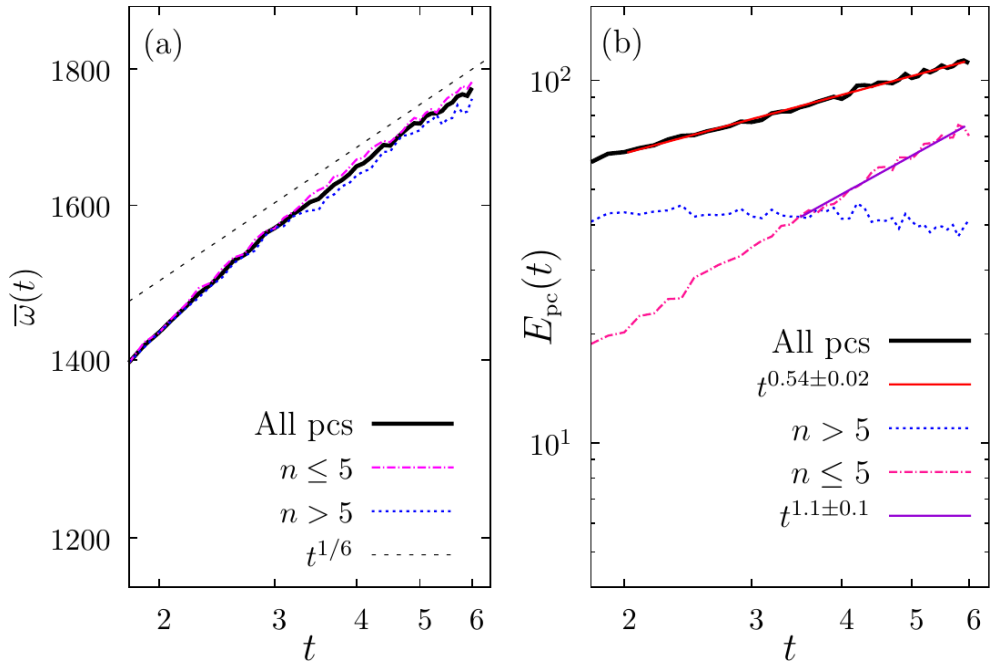

FIG. 9. (a) Vortex mean vorticity $\overline{\omega}(t)$ of vortices in all perfectly polarized clusters ("All pcs," solid black line), small clusters with $n \leqslant 5$ vortices (dash-dot magenta line), and large clusters with $n > 5$ vortices (dotted blue line). Also shown is a $t^{1/6}$ scaling line (dashed black). (b) Total kinetic energy in all perfect clusters ("All pcs," solid black line) with least-squares fit line (solid red) $t^{0.54\pm0.02}$ over $2.0 \leqslant t \leqslant 6.0$, in large clusters with $n > 5$ vortices (dotted blue line), and in small clusters with $n \leqslant 5$ vortices (dash-dot magenta line) with least-squares fit line (solid violet) $t^{1.1\pm0.1}$ over $3.5 \leqslant t \leqslant 6.0$.

clusters to be estimated as

$$A_{\rm pc} = N_{\rm v}^{\rm pc} \ell^2(t) = 4\pi^2 N_{\rm v}^{\rm pc} E_{\rm pc}/Z_{\rm v}^{\rm pc}. \tag{12}$$

In Fig. 10 the area $A_{\rm pc}$ occupied by perfect clusters with n vortices, where n is given in the legend, is plotted as a function of $4\pi^2 N_{\rm v}^{\rm pc} E_{\rm pc}/Z_{\rm v}^{\rm pc}$ at times $3.0 \leqslant t \leqslant 6.0$. A least-squares best fit (solid black line) yields exponent 0.89 ± 0.04, and the theoretical prediction (dotted black line) of Eq. (12) is shown for comparison. The mean-field prediction underestimates the total cluster area for all n, which is not surprising because in this forced-dissipative flow the forcing continually replenishes an incoherent "sea" of vorticity. This "sea" is more diffuse and occupies a larger area than the vortex cores, and is not accounted for in $N_{\rm v}^{\rm pc}$. In general, however, the observed relationship is close to the prediction of Eq. (12). This result supports interpreting $\ell^2(t)$ as an area associated with the vortex, but extending beyond its core.

Assuming $\ell^2(t) \sim \overline{A}(t)$ allows a separate mean-field prediction for the cluster energy,

$$E_{\rm pc} \sim N_{\rm v}^{\rm pc} \frac{\overline{\Gamma}^2(t)}{\mathcal{D}}, \tag{13}$$

where $\mathcal{D}$ is the area of the domain. This is the expression for the mean-field energy used by Carnevale *et al.* [30] and LaCasce [25]. To predict how the mean-field energy $E_{\rm pc}$ given by Eq. (13) will grow in time requires the time-dependence of $N_{\rm v}^{\rm pc}$, $\overline{A}(t)$ and $\overline{\omega}(t)$ to be specified. The mean-field theories developed by previous authors were semiempirical: Carnevale *et al.* [30] relied on numerical simulations to determine the density decay exponent, and LaCasce [25] appealed to the measured growth rate of the mean vortex circulation and diffusivity. The mean-field theory

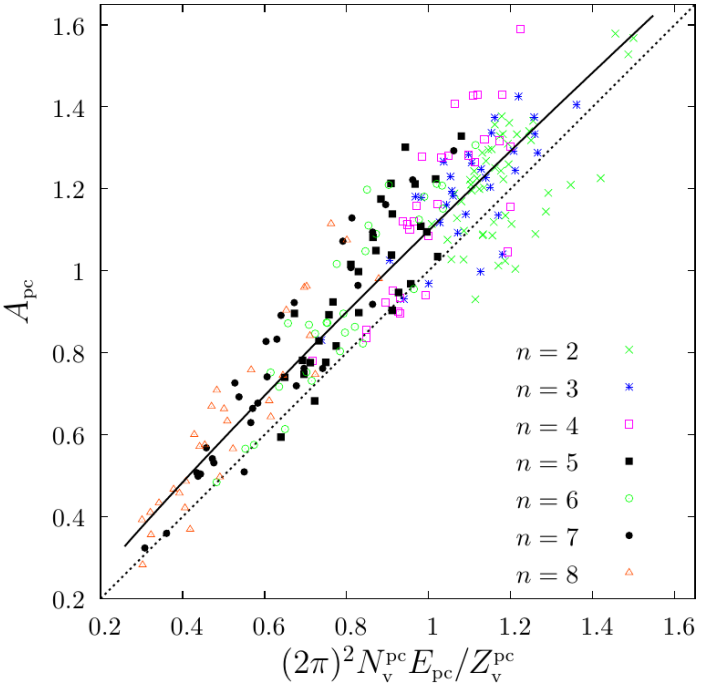

FIG. 10. Total area $A_{\rm pc}$ occupied by clusters with n vortices, where $n \in 2, 3, \ldots, 8$, plotted as a function of $4\pi^2 N_{\rm v}^{\rm pc} E_{\rm pc}/Z_{\rm v}^{\rm pc}$ for $3.0 \leqslant t \leqslant 6.0$. (Different points correspond to different times.) Also shown are a least-squares best fit $A_{\rm pc} = [4\pi^2 N_{\rm v}^{\rm pc} E_{\rm pc}/Z_{\rm v}^{\rm pc}]^{0.89\pm0.04}$ (solid black line) and the mean-field theoretical prediction (dotted black line).

developed here will also rely on several empirical observations. As shown in Fig. 9(a), in these simulations $\overline{\omega}(t) \sim t^{1/6}$ after $t \approx 3.5$. The vortex mean vorticity most likely grows because small intense vortices injected into the incoherent flow by the forcing are scavenged up by large coherent vortices. There may also be a contribution from hyperviscous sharpening of the vortex peak [17].

Burgess and Scott [16] predicted $N_{\rm v} \sim t^{-1}$ in the A^{-1} range. The observed decay rate of the number of clustered vortices $N_{\rm v}^{\rm pc}$ is faster than this, as shown in Fig. 6(a), but for the purposes of developing the theory it will be assumed that $N_{\rm v}^{\rm pc} \sim t^{-1}$. As shown in Fig. 3(b) and as expected for the A^{-1} range, which is enstrophy-conserving, total coherent enstrophy $Z_{\rm v}^{\rm pc}$ is conserved by the clustered vortices after $t \approx 2.0$,

$$Z_{\rm v}^{\rm pc} = N_{\rm v}^{\rm pc} \overline{A}(t) \overline{\omega_{\rm v}^2}(t) \sim t^{-1} \overline{A}(t) t^{1/3} = \text{constant}, \tag{14}$$

from which it immediately follows that

$$\overline{A}(t) \sim t^{2/3}. \tag{15}$$

As shown in Fig. 6(d) (black dash-dot curve with magenta fit) the mean vortex area $\overline{A}(t) \sim t^{0.67\pm0.01}$ in perfectly polarized clusters. Using Eq. (13) it also follows that

$$E_{\rm pc} \sim t^{2/3}. \tag{16}$$

As shown in Fig. 9(b) the total energy $E_{\rm pc}$ in perfect clusters (solid black line) follows a clean power law and grows more slowly than predicted by Eq. (16), with $E_{\rm pc} \propto t^{0.54\pm0.02}$ (red least-squares best fit line) over $2.0 \leqslant t \leqslant 6.0$. As will be shown below, the prediction given by Eqs. (13) and (16) for $E_{\rm pc}$ differs from what is observed because vortices in small and large perfect clusters exhibit different statistics: their mean core areas $\overline{A}(t)$ grow at different rates, and their number and total

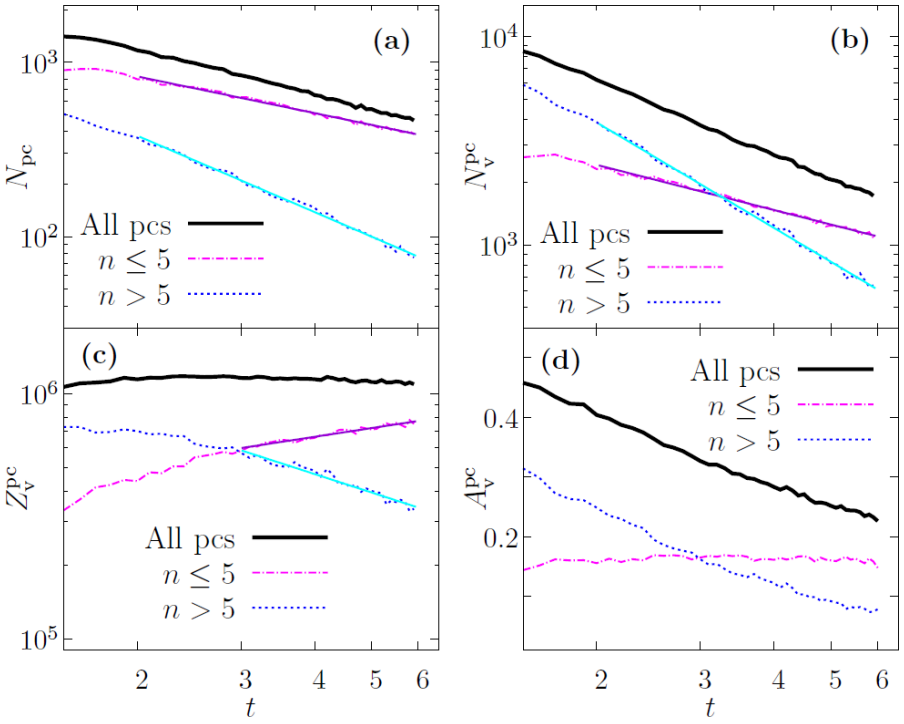

FIG. 11. (a) Number $N_{\rm pc}$ of perfect clusters ("All pcs," solid black line), perfect clusters with $n \leqslant 5$ vortices (dash-dot magenta line), and perfect clusters with $n > 5$ vortices (dotted blue line). Also shown are least-squares best fit lines $t^{-0.70\pm0.04}$ (solid violet) and $t^{-1.45\pm0.06}$ (solid cyan) over $2.0 \leqslant t \leqslant 6.0$. (b) Number of vortices $N_{\rm v}^{\rm pc}$ in all perfect clusters (solid black line), in perfect clusters with $n \leqslant 5$ vortices (dash-dot magenta line), and in perfect clusters with $n > 5$ vortices (dotted blue line). Also shown are best fit lines $t^{-0.72\pm0.04}$ (solid violet) and $t^{-1.68\pm0.06}$ (solid cyan) over $2.0 \leqslant t \leqslant 6.0$. (c) Total coherent enstrophy $Z_{\rm v}^{\rm pc}$ in all perfect clusters (solid black line), clusters with $n \leqslant 5$ vortices (dash-dot magenta line), and clusters with $n > 5$ vortices (dotted blue line). Also shown are least-squares best fit lines $t^{0.35\pm0.07}$ (solid violet) and $t^{-0.8\pm0.1}$ (solid cyan) over $3.0 \leqslant t \leqslant 6.0$. (d) Total coherent area $A_{\rm v}^{\rm pc}$ in all perfect clusters (solid black line), in perfect clusters with $n \leqslant 5$ vortices (dash-dot magenta line), and in perfect clusters with $n > 5$ vortices (dotted blue line).

coherent enstrophy follow different power laws, as shown in Fig. 11. While the vortices in small clusters are the largest and strongest in the flow and dominate $\overline{A}(t)$, the larger clusters make the dominant contribution to $E_{\rm pc}$ up to $t \approx 3.5$, as can be seen by comparing the dotted blue line (energy in large clusters) to the dash-dot magenta line (energy in small clusters) in Fig. 9(b). Consequently $\ell^2(t) \propto \overline{A}(t)$, a crucial assumption made in arriving at Eq. (13), when $\ell(t)$ is computed from Eq. (9) using the energy and coherent enstrophy contained in all perfectly polarized clusters regardless of size. As a result, the above mean-field argument, when applied to the entire clustered population, simultaneously predicts the correct growth law for $\overline{A}(t)$ and overestimates the growth rate of $E_{\rm pc}$.

A. A mean-field theory for small clusters

A consistent mean-field theory for the vortices in perfectly polarized clusters must treat small and large clusters separately. This is evident from Fig. 11, which shows that small and large clusters exhibit markedly different scaling behavior, which also differs from the clustered population as a whole. In Fig. 11 the threshold number of vortices separating small from large clusters has been set to $n_{\rm thr} = 5$, a choice that will be motivated below. As shown in Fig. 11(a) the number $N_{\rm pc}$ of small clusters with 5 or fewer vortices ($n \leqslant 5$, magenta dash-dot line) exceeds the number of large

clusters with 5 or more vortices ($n > 5$, dotted blue line) at all times, and decays more slowly. The faster decrease in the number of large clusters is consistent with the faster decay in their total number of vortices N_v^{pc} as shown in Fig. 11(b), dotted blue line, and with the decay in their total coherent enstrophy Z_v^{pc}, Fig. 11(c), dotted blue line. In contrast, the total coherent enstrophy Z_v^{pc} in small clusters with 5 or fewer vortices ($n \leqslant 5$, dash-dot magenta line) grows, dominating the coherent enstrophy in large clusters ($n > 5$, dotted blue line) after $t \approx 3.0$. The measured power-law exponents (violet and cyan least-squares best fit lines) for the quantities in Fig. 11 will be discussed below in the context of developing a mean-field theory for small clusters.

Figure 11(d) shows the total coherent area (i.e., area occupied by vortex cores) A_v^{pc} in all perfectly polarized clusters (solid black line), in small clusters ($n \leqslant 5$, dash-dot magenta line), and in large clusters ($n > 5$, dotted blue line). Interestingly, the total coherent area in small clusters is approximately conserved and dominates the coherent area in large clusters after $t \approx 3.0$. In contrast the total coherent area in large perfect clusters decays.

To proceed with a mean-field theory that treats small and large clusters separately it is necessary to choose a threshold number of vortices n_{thr} distinguishing small from large clusters. Guidance on this matter may be obtained by considering the relative decay rates of the number of large versus small clusters, shown in Fig. 11, taking $n_{thr} = 5$ for illustration. As discussed above, the number of large clusters decreases more quickly than the number of small clusters. This indicates that large perfect clusters are preferentially disassembled by the vortex motions, while small clusters decrease in number more slowly. This may be because small perfect clusters are closer to stable equilibrium configurations, such as like-sign pairs and triangles [42], and therefore persist longer, while large groups of like-sign vortices are more unstable and come apart more quickly.

A natural way to divide the clusters is to seek a range of cluster sizes not affected by this preferential disassembly, whose number decreases at a rate roughly independent of the number of vortices in the cluster, and to label these clusters "small." If the decay rate of the number of clusters is independent of cluster size (i.e., number of vortices n) over a certain range, then the number of vortices per cluster should be constant when computed over this range. Conversely, if the largest clusters in the selected range are preferentially disassembled, the number of vortices per cluster should decrease. This offers a way of selecting a range of cluster sizes: a reasonable criterion is that "small clusters" be selected so that the number of vortices per cluster is constant over the course of the simulation. The number of vortices per cluster N_v^{pc}/N_{pc} for several choices of n_{thr} is shown in Fig. 12(a). When clusters with up to 8 vortices are included ($n \leqslant n_{thr}$, $n_{thr} = 8$, solid black curve), the number of vortices per cluster N_v^{pc}/N_{pc} decreases significantly from its initial value of 3.6, with a final value of about 3.3 by $t = 6.0$. Smaller decreases are seen for $n_{thr} = 7$ (double-dotted green curve) and $n_{thr} = 6$ (dotted blue curve), but for the latter choice of n_{thr} the decay is still from an initial value $N_v^{pc}/N_{pc} \approx 3.15$ to a final value $N_v^{pc}/N_{pc} \approx 3.0$. For clusters with 5 or fewer vortices ($n_{thr} = 5$, dash-dot magenta line) the decay is much less marked, from an initial value of $N_v^{pc}/N_{pc} \approx 2.9$ to a final value of $N_v^{pc}/N_{pc} \approx 2.85$. This much slower decay motivates a choice of cutoff $n_{thr} = 5$.

How the decay rate of the number of clusters depends on n, the number of vortices in the cluster, can also be tested directly by plotting N_{pc} as a function of time t for various choices of n, as is done in Fig. 12(b) for $n \in 2, 3, 4, 5$. The number of clusters with 2 vortices ($n = 2$, solid dark orange line) and 3 vortices ($n = 3$, double-dotted violet line) both decay at a rate close to $t^{-2/3}$, with $N_{pc} \sim t^{-0.66\pm0.05}$ (solid dark orange least-squares fit line) for 2 vortices and $N_{pc} \sim t^{-0.69\pm0.07}$ (solid violet least-squares fit line) for 3 vortices. The number of clusters with 4 and 5 vortices (dotted red and dash-dot royal blue lines) decay more steeply, but the uncertainty is large, with least-squares best fits yielding $t^{-0.81\pm0.09}$ (solid red line) and $t^{-0.8\pm0.1}$ (royal blue line). For clusters with 6 vortices (not shown) the decay rate jumps to $N_{pc} \sim t^{-1.0\pm0.1}$, and the number of clusters with 7 and with 8 vortices decay more steeply, like $t^{-1.2\pm0.2}$ and $t^{-1.3\pm0.2}$. Larger clusters decay at even steeper rates, though the uncertainties are large due to low cluster numbers and large fluctuations.

To proceed, note that after $t \approx 3.0$ vortices in small perfect clusters make the dominant contribution to both N_v^{pc} in Fig. 11(b) and to the total coherent area A_v^{pc} in Fig. 11(d), so it is reasonable to expect that they will also dominate $\overline{A}(t)$, and that consequently $\overline{A}(t) \sim t^{2/3}$ will still hold when

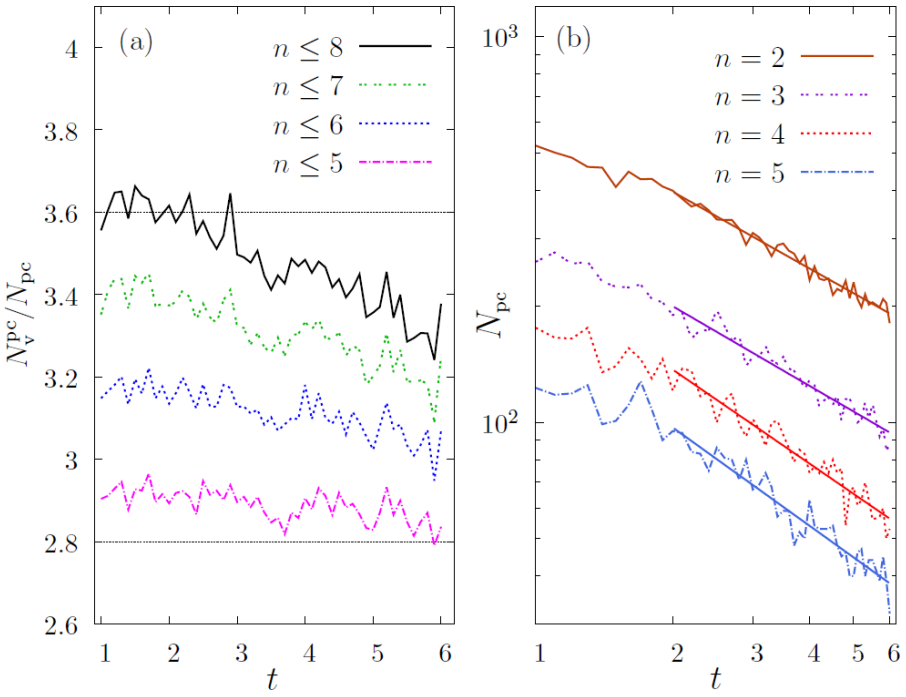

FIG. 12. (a) Number of vortices per cluster as a function of time t for clusters containing $n \leqslant 8$ vortices (solid black line), $n \leqslant 7$ vortices (double-dotted green line), $n \leqslant 6$ vortices (dotted blue line), and $n \leqslant 5$ vortices (magenta dash-dot line). (b) Number of clusters $N_{\rm cl}$ with 2 vortices (solid dark orange line), 3 vortices (double-dotted violet line), 4 vortices (dotted red line), and 5 vortices (dash-dot royal blue line) as functions of time t together with least-squares best fits over $2.0 \leqslant t \leqslant 6.0$, from top to bottom, $t^{-0.66\pm0.05}$ (solid dark orange), $t^{-0.69\pm0.07}$ (solid violet), $t^{-0.81\pm0.09}$ (solid red), and $t^{-0.8\pm0.1}$ (solid royal blue).

the computation is restricted to vortices in small clusters. As shown in Fig. 13(a) this is indeed the case: for clusters with $n \leqslant 5$ vortices $\overline{A}(t) \sim t^{0.69\pm0.03}$ (magenta dash-dot curve with solid violet fit line) over the interval $3.0 \leqslant t \leqslant 6.0$. In contrast, for larger clusters with $n > 5$ vortices the mean vortex area grows more slowly, with $\overline{A}(t) \sim t^{0.49\pm0.03}$ (dotted blue curve with solid cyan fit line). As shown in Fig. 9(a) the measured growth of $\overline{\omega}(t)$, is almost the same for the clustered vortex population as a whole (solid black line) and the vortices in large (dotted blue) and small (dash-dot magenta) clusters considered separately, and is approximately $t^{1/6}$ after $t \approx 3.5$, though note that the growth at earlier times is steeper and does not follow a power law. The shared growth rate suggests that forcing effects, which impact all vortices, primarily cause this growth.

Combining the assumption that vortices in small clusters dominate the growth rate of the mean vortex area, such that $\overline{A}(t) \sim t^{2/3}$ for small clusters, with the empirical observations that $\overline{\omega}^2(t) \sim t^{1/3} \sim \overline{\omega_{\rm v}^2}$ and that the coherent area $A_{\rm v}^{\rm pc}$ in small clusters is roughly constant it is possible to predict the time-dependence of the total number $N_{\rm v}^{\rm pc}$ of vortices, the total coherent enstrophy $Z_{\rm v}^{\rm pc}$, and the total kinetic energy $E_{\rm pc}$ in small clusters. Constancy of the coherent area and $\overline{A}(t) \sim t^{2/3}$ together yield

$$A_{\rm v}^{\rm pc} = N_{\rm v}^{\rm pc}(t)\overline{A}(t) = \text{constant} \quad \Rightarrow N_{\rm v}^{\rm pc}(t) \sim t^{-2/3}. \tag{17}$$

A least-squares best fit (solid violet line) to the total number of vortices in small clusters, Fig. 11(b), yields $N_{\rm v}^{\rm pc} \sim t^{-0.72\pm0.04}$. This is somewhat faster than predicted, consistent with the faster decrease in the number of clusters with $n = 4$ and $n = 5$ vortices as compared to $n = 2$ and $n = 3$

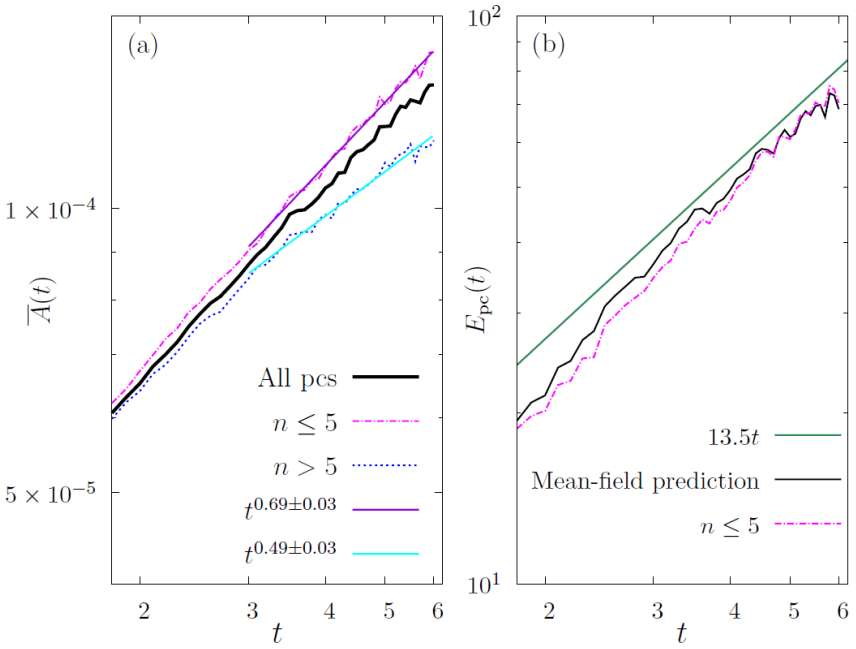

FIG. 13. (a) Mean area of a clustered vortex taken over all clusters (solid black line), clusters with 5 or fewer vortices (dash-dot magenta line), and clusters with 5 or more vortices (dashed blue line), with best fit lines (solid violet and cyan) over $3.0 \leqslant t \leqslant 6.0$. (b) Energy $E_{\rm pc}(t)$ in perfect clusters with $n \leqslant 5$ vortices (dash-dot magenta line), mean-field prediction $E_{\rm pc}(t) \sim \mathcal{D}^{-1} N_{\rm v}^{\rm pc} \overline{A}^2(t) \overline{\omega_{\rm v}^2}$ (solid black line) from Eq. (20), and t scaling line (solid sea-green).

vortices—see Fig. 12(b). Assuming the number of vortices per cluster is constant then leads to

$$N_{\rm pc}(t) \sim N_{\rm v}^{\rm pc}(t) \sim t^{-2/3}. \tag{18}$$

A least-squares best fit (solid violet) to the number of small clusters (magenta dash-dot line) in Fig. 11(a) yields $N_{\rm pc} \sim t^{-0.70\pm0.04}$, which is $t^{2/3}$ to within the error bars.

Using the constancy of the coherent area together with $\overline{\omega_{\rm v}^2} \sim t^{1/3}$ yields the growth rate of the total coherent enstrophy in small clusters,

$$Z_{\rm v}^{\rm pc}(t) = A_{\rm v}^{\rm pc} \overline{\omega_{\rm v}^2}(t) \sim t^{1/3}. \tag{19}$$

A least-squares best fit line (violet) to the magenta dash-dot line in Fig. 11(c) yields $Z_{\rm v}^{\rm pc}(t) \sim t^{0.35\pm0.07}$ over $3.0 \leqslant t \leqslant 6.0$, verifying this prediction.

Finally, assuming $\ell^2(t) \sim \overline{A}(t) \sim t^{2/3}$ for the vortices in small perfect clusters yields

$$E_{\rm pc}(t) \sim \mathcal{D}^{-1} N_{\rm v}^{\rm pc} \overline{A}^2(t) \overline{\omega_{\rm v}^2} \sim t. \tag{20}$$

As shown in Fig. 9(b) the energy in small clusters (dash-dot magenta curve) grows like $t^{1.1\pm0.1}$ (solid violet least-squares fit line), where the fit is over the range of times ($3.5 \leqslant t \leqslant 6.0$) for which $\overline{\omega_{\rm v}^2}$ is roughly constant—see Fig. 9(a).

In Fig. 13(b) the measured growth of the energy $E_{\rm pc}(t)$ in small clusters (dash-dot magenta line) is further compared with the mean-field prediction $\mathcal{D}^{-1} N_{\rm v}^{\rm pc} \overline{A}^2(t) \overline{\omega_{\rm v}^2}$ (solid black line) from Eq. (20). In general, the agreement is very good. The mean-field prediction slightly overestimates $E_{\rm pc}$ up until $t \approx 4.5$, and its growth rate is closer to t, as can be seen by comparing to the t scaling line (sea-green). At late times, $4.5 \leqslant t \leqslant 6.0$, the mean-field and measured $E_{\rm pc}$ agree almost exactly,

showing the power of the mean-field approach for small clusters once the vortex population is well-developed.

VIII. DISCUSSION AND CONCLUSIONS

The results discussed above show that the inverse energy cascade in forced-dissipative two-dimensional turbulence involves two processes: the concentration of a constant amount of coherent enstrophy into a smaller and smaller fraction of the domain, and the simultaneous randomization of the surrounding flow, as evidenced by decreasing polarization of the vortex population outside the perfect clusters. Vortices in perfectly polarized clusters conserve their coherent enstrophy. As merger generates larger and larger vortices, perfectly polarized clusters simultaneously become more widely spaced, and this conserved enstrophy is concentrated into an ever-shrinking area. At the same time there is growing disorder in the vortex population outside the perfect clusters, as evidenced by the preferential disassembly of the larger perfect clusters and decreasing polarization of the surrounding flow. This "spreading neutralization," which eats away at the perfect clusters as the inverse cascade proceeds, might suggest that the vortex population is undergoing statistical cooling in the sense of Onsager [43,44], i.e., moving toward a state dominated by dipoles rather than like-sign clusters. However, the question of statistical heating or cooling of the population is subtle. Firstly, there is no clean mapping between this forced-dissipative system and the freely evolving system of point vortices considered by Onsager. In the forced-dissipative system the coherent vortices are surrounded by an incoherent sea of filamentary vorticity, which is constantly replenished by the forcing, and which is absent from the point vortex system. This sea interacts with the coherent vortices and with itself, making contributions to the energy that are not represented in the point vortex system considered by Onsager. Furthermore, in the forced-dissipative system energy grows continually, whereas the point vortex system considered by Onsager is energy-conserving. As the energy grows in the forced-dissipative system, the available microstates continually change. It is thus not immediately clear how to apply Onsager's theory to the vortex population in forced-dissipative two-dimensional turbulence. Furthermore, merger can counterintuitively lead to weak statistical heating, as shown by Esler and Scott [44] for vortices in freely decaying two-dimensional turbulence. Hence, no conclusions regarding statistical heating or cooling are drawn here for the forced-dissipative vortex population on the basis of the present evidence.

In conclusion, this paper sheds light on how long-lived vortices in the inverse cascade of forced-dissipative two-dimensional turbulence are organized in the domain and how this organization relates to the multirange power-law scaling behavior seen in their number density distribution. The notion of a perfectly polarized cluster, the largest possible region bounded by a level set of the stream function and containing vortices of only one sign, was introduced. Perfect clusters almost fill the domain at early times, containing most of the system's energy and enstrophy, but become more widely separated as like-sign merger generates larger and fewer vortices, which more sparsely populate the domain.

The number density distributions of free vortices and vortices in perfect clusters differ significantly in their scaling behavior. The free number density has an equilibrated range stretching from small to intermediate scales in which $n_{\mathrm{f}}(A,t) \sim A^{-3}$. The clustered number density, however, has a nonequilibrated range at intermediate scales with a scale-invariant distribution of areas, $n_{\mathrm{pc}}(A,t) \sim A^{-1}$, and the number of vortices falls off in time through merger and ejection of vortices into the free population. The A-dependence of the small- and intermediate-scale ranges observed in the full number density [16] is thus associated with vortices in different parts of the flow, the small-scale A^{-3} range with free vortices, and the intermediate-scale A^{-1} range with clustered vortices. Allowing the clusters to contain some vortices of the opposite sign results in progressive loss of the A^{-1} scaling as the polarization threshold is relaxed, confirming that this scale-invariant area distribution is associated with like-sign vortices in perfectly polarized clusters.

A mean-field argument using the conservation of coherent enstrophy by vortices in perfect clusters, the theoretically predicted decay rate of their number, and the observed growth rate of vortex

mean-square vorticity correctly predicts how the mean area of a clustered vortex grows in time, but incorrectly predicts the growth rate of the energy in perfect clusters. This is because vortices in small clusters exhibit different statistics than vortices in large clusters, which are undergoing preferential disassembly. Small clusters are likely closer to stable equilibrium configurations, which may account for their ability to persist longer than large clusters, which are more unstable and prone to coming apart.

Vortices in small perfectly polarized clusters conserve their total coherent area, and using this fact along with the growth rates of the vortex mean-square vorticity and average vortex area allows a semiempirical mean-field theory to be developed for these vortices. This theory successfully predicts the time-dependence of the coherent enstrophy and kinetic energy contained in small perfect clusters, the number of small clusters, and the number of clustered vortices. At late times the mean-field and observed energies agree almost exactly, showing the power of the mean-field approach for small clusters.

Though the present work provides new insight into the spatial organization of the flow and how it relates to scaling in the vortex population, it leaves untouched the question of what types of interactions occur between vortices to generate the scaling ranges and drive exchanges between the free and clustered populations. To fully understand the number density and its conservation properties it is necessary to study vortex interactions, including exchanges between the clustered and free populations. The clusters and scaling behavior studied here are also expected to be transient since the system will eventually enter a condensation regime, which will no doubt change the spatial organization and properties of the vortices. This and other questions will be addressed in subsequent work.

ACKNOWLEDGMENT

B.H.B. acknowledges support from a Leverhulme Early Career Fellowship [Award No. ECF-2017-508].

[1] J. C. McWilliams, The emergence of isolated coherent vortices in turbulent flow, J. Fluid Mech. **146**, 21 (1984).
[2] R. Benzi, S. Patarnello, and P. Santangelo, On the statistical properties of two-dimensional decaying turbulence, Europhys. Lett. **3**, 811 (1987).
[3] R. Benzi, S. Patarnello, and P. Santangelo, Self-similar coherent structures in two-dimensional decaying turbulence, J. Phys. A: Math. Gen. **21**, 1221 (1988).
[4] P. Santangelo, R. Benzi, and B. Legras, The generation of vortices in high resolution, two-dimensional decaying turbulence and the influence of initial conditions on the breaking of self-similarity, Phys. Fluids A **1**, 1027 (1989).
[5] J. C. McWilliams, The vortices of two-dimensional turbulence, J. Fluid Mech. **219**, 361 (1990).
[6] J. B. Weiss and J. C. McWilliams, Temporal scaling behaviour of decaying two-dimensional turbulence, Phys. Fluids A **5**, 608 (1993).
[7] V. Borue, Inverse Energy Cascade in Stationary Two-Dimensional Homogeneous Turbulence, Phys. Rev. Lett. **72**, 1475 (1994).
[8] L. M. Smith and V. Yakhot, Finite-size effects in forced two-dimensional turbulence, J. Fluid Mech. **274**, 115 (1994).
[9] S. Danilov and D. Gurarie, Forced two-dimensional turbulence in spectral and physical space, Phys. Rev. E **63**, 061208 (2001).
[10] R. K. Scott, Nonrobustness of the two-dimensional inverse cascade, Phys. Rev. E **75**, 046301 (2007).
[11] A. Vallgren, Infrared Reynolds number dependency of the two-dimensional inverse energy cascade, J. Fluid Mech. **667**, 463 (2011).

[12] J. Fontane, D. G. Dritschel, and R. K. Scott, Vortical control of forced two-dimensional turbulence, Phys. Fluids **25**, 015101 (2013).
[13] B. H. Burgess, R. K. Scott, and T. G. Shepherd, Kraichnan-Leith-Batchelor similarity theory and two-dimensional inverse cascades, J. Fluid Mech. **767**, 467 (2015).
[14] D. G. Dritschel, R. K. Scott, C. Macaskill, G. A. Gottwald, and C. V. Tran, Unifying Scaling Theory for Vortex Dynamics in Two-Dimensional Turbulence, Phys. Rev. Lett. **101**, 094501 (2008).
[15] B. H. Burgess, D. G. Dritschel, and R. K. Scott, Extended scale invariance in the vortices of freely evolving two-dimensional turbulence, Phys. Rev. Fluids **2**, 114702 (2017).
[16] B. H. Burgess and R. K. Scott, Scaling theory for vortices in the two-dimensional inverse energy cascade, J. Fluid Mech. **811**, 742 (2017).
[17] B. H. Burgess and R. K. Scott, Robustness of vortex populations in the two-dimensional inverse energy cascade, J. Fluid Mech. **850**, 844 (2018).
[18] R. Benzi, M. Colleta, M. Briscolini, and P. Santangelo, A simple point vortex model of two-dimensional decaying turbulence, Phys. Fluids A **4**, 1036 (1992).
[19] E. Trizac, A Coalescence Model for Freely Decaying Two-Dimensional Turbulence, Europhys. Lett. **43**, 671 (1998).
[20] A. Bracco, J. C. McWilliams, G. Murate, A. Provenzale, and J. B. Weiss, Revisiting freely decaying two-dimensional turbulence at millenial resolution, Phys. Fluids **12**, 2931 (2000).
[21] H. J. H. Clercx and A. H. Nielsen, Vortex Statistics for Turbulence in a Container with Rigid Boundaries, Phys. Rev. Lett. **85**, 752 (2000).
[22] C. Sire and P.-H. Chavanis, Numerical renormalization group of vortex aggregation in two-dimensional turbulence: The role of three-body interactions, Phys. Rev. E **61**, 6644 (2000).
[23] H. J. H. Clercx, G. J. F. van Heijst, and M. L. Zoeteweij, Quasi-two dimensional turbulence in shallow fluid layers: The role of bottom friction and fluid layer depth, Phys. Rev. E **67**, 066303 (2003).
[24] L. J. A. van Bokhoven, R. R. Trieling, H. J. H. Clercx, and G. J. F. van Heijst, Influence of initial conditions on decaying two-dimensional turbulence, Phys. Fluids **19**, 046601 (2007).
[25] J. H. LaCasce, The vortex merger rate in freely decaying, two-dimensional turbulence, Phys. Fluids **20**, 085102 (2008).
[26] P. Tabeling, S. Burkhart, O. Cardoso, and H. Willaime, Experimental Study of Freely Decaying Two-Dimensional Turbulence, Phys. Rev. Lett. **67**, 3772 (1991).
[27] O. Cardoso, D. Marteau, and P. Tabeling, Quantitative experimental study of the free decay of quasi-two-dimensional turbulence, Phys. Rev. E **49**, 454 (1994).
[28] A. E. Hansen, D. Marteau, and P. Tabeling, Two-dimensional turbulence and dispersion in a freely decaying system, Phys. Rev. E **58**, 7261 (1998).
[29] G. F. Carnevale, Y. Pomeau, and W. R. Young, Statistics of Ballistic Agglomeration, Phys. Rev. Lett. **64**, 2913 (1990).
[30] G. F. Carnevale, J. C. McWilliams, Y. Pomeau, J. B. Weiss, and W. R. Young, Evolution of Vortex Statistics in Two-Dimensional Turbulence, Phys. Rev. Lett. **66**, 2735 (1991).
[31] G. Huber and P. Alström, Universal decay of vortex density in two dimensions, Physica A **195**, 448 (1993).
[32] E. Trizac and J.-P. Hansen, Dynamics and growth of particles undergoing ballistic aggregation, J. Stat. Phys. **82**, 1345 (1996).
[33] Y. Pomeau, Vortex dynamics in perfect fluids, J. Plasma Phys. **56**, 407 (1996).
[34] T. Iwayama, H. Fujisaka, and H. Okamoto, Phenomenological determination of scaling exponents in two-dimensional decaying turbulence, Prog. Theor. Phys. **98**, 1219 (1997).
[35] B. H. Burgess, D. G. Dritschel, and R. K. Scott, Vortex scaling ranges in two-dimensional turbulence, Phys. Fluids **29**, 111104 (2017).
[36] T. Y. Hou and R. Li, Dynamic depletion of vortex stretching and non-blowup of the 3D incompressible euler equations, J. Nonlin. Sci. **16**, 639 (2006).
[37] P. Bartello and T. Warn, Self-similarity of decaying two-dimensional turbulence, J. Fluid Mech. **326**, 357 (1996).
[38] D. G. Dritschel and D. W. Waugh, Quantification of the inelastic interaction of unequal vortices in two-dimensional vortex dynamics, Phys. Fluids A **4**, 1737 (1992).

[39] F. Vega-Redondo, Mean-field theory, in *Complex Social Networks*, Econometric Society Monographs (Cambridge University Press, Cambridge, UK, 2007), pp. 268–274.
[40] R. H. Kraichnan, Statistical dynamics of two-dimensional flow, J. Fluid Mech. **67**, 155 (1975).
[41] A. F. Thompson and W. R. Young, Scaling baroclinic eddy fluxes: Vortices and energy balance, J. Phys. Oceanogr. **36**, 720 (2006).
[42] H. Aref, Motion of three vortices, Phys. Fluids **22**, 393 (1979).
[43] L. Onsager, Statistical hydrodynamics, Nuovo Cim. **6**, 279 (1949).
[44] J. G. Esler and R. K. Scott, Decaying two-dimensional turbulence undergoes statistical heating, Phys. Rev. Fluids **5**, 074601 (2020).